Biophysical Chemistry 168–169 (2012) 28–39

Contents lists available at SciVerse ScienceDirect

Biophysical Chemistry

journal homepage: http://www.elsevier.com/locate/biophyschem

Rotational velocity rescaling of molecular dynamics trajectories for direct prediction of protein NMR relaxation

Janet S. Anderson [a], David M. LeMaster [b,*]

[a] Department of Chemistry, Union College, Schenectady, NY, 12308, United States
[b] Wadsworth Center, New York State Department of Health and Department of Biomedical Sciences, School of Public Health, University at Albany — SUNY, Empire State Plaza, Albany, NY, 12201, United States

HIGHLIGHTS

- Rescaling of rotational velocity in molecular dynamics for the B3 domain of Protein G reproduces its anisotropic tumbling.
- The optimal rotational velocity rescaling factor closely matches that predicted from the self-diffusion rate of TIP3P water.
- ^{15}N relaxation data of GB3 can be predicted from the rescaled trajectories with no system-specific adjustable parameters.
- ^{15}N chemical shift anisotropy of −168 ppm predicts the field-dependent data better than reported residue-specific values.
- Sites for which observed and predicted relaxation markedly differ are assessed in terms of implied force field inadequacies.

GRAPHICAL ABSTRACT

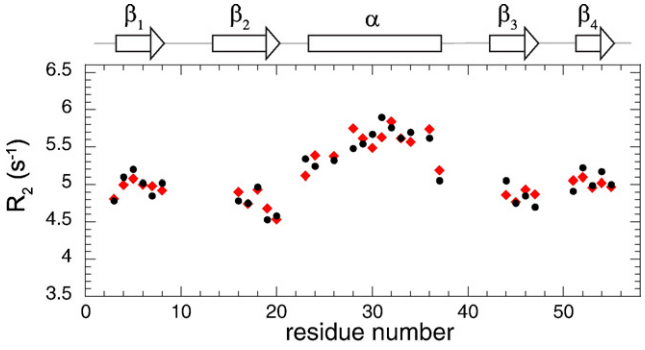

ARTICLE INFO

Article history:
Received 29 April 2012
Received in revised form 28 May 2012
Accepted 31 May 2012
Available online 7 June 2012

Keywords:
Molecular dynamics simulation
NMR relaxation
Rotational diffusion

ABSTRACT

Rotational velocity rescaling (RVR) enables ^{15}N relaxation data for the anisotropically tumbling B3 domain of Protein G (GB3) to be accurately predicted from 1 μs of constant energy molecular dynamics simulation without recourse to any system-specific adjustable parameters. Superposition of adjacent trajectory frames yields the unique rotation axis and angle of rotation that characterizes each transformation. By proportionally scaling the rotation angles relating each consecutive pair of frames, the rotational diffusion in the RVR-MD trajectory was adjusted to correct for the elevated self-diffusion rate of TIP3P water. ^{15}N T_1 and T_2 values for 32 residues in the regular secondary structures of GB3 were predicted with an rms deviation of 2.2%, modestly larger than the estimated experimental uncertainties. Residue-specific chemical shift anisotropy (CSA) values reported from isotropic solution, liquid crystal and microcrystalline solid measurements less accurately predict GB3 relaxation than does applying a constant CSA value, potentially indicating structure-dependent correlated variations

Abbreviations: RVR, rotational velocity rescaling; GB3, B3 domain of Protein G; PDB, protein data bank; MD, molecular dynamics; rms, root mean square; RDC, residual dipolar coupling; NOE, nuclear Overhauser enhancement; CSA, chemical shift anisotropy; ROESY, rotating frame nuclear Overhauser enhancement spectroscopy.

* Corresponding author at: Wadsworth Center, New York State Department of Health and Department of Biomedical Sciences, School of Public Health, University at Albany — SUNY, Empire State Plaza, Albany, New York, 12201, United States. Tel.: +1 518 474 6396; fax: +1 518 473 2900.
E-mail address: lemaster@wadsworth.org (D.M. LeMaster).

0301-4622/$ – see front matter
doi:10.1016/j.bpc.2012.05.005

in $^{1}H-^{15}N$ bond length and ^{15}N CSA. By circumventing the quasi-static analysis of NMR order parameters often applied in MD studies, a more direct test is provided for assessing the accuracy with which molecular simulations predict protein motion in the ps–ns timeframe. Since no assumption of separability between global tumbling and internal motion is required, utility in analyzing simulations of mobility in disordered protein segments is anticipated.

1. Introduction

NMR relaxation measurements provide experimental monitors of protein conformational dynamics with an atomic level of detail that is unmatched by any other technique. As such, in principle, relaxation experiments offer the most stringent test available for assessing the accuracy with which molecular dynamics simulations model the rates of intramolecular motion that occurs in proteins and biomacromolecules in general. In practice, nearly all comparisons between MD predictions and observed protein NMR relaxation behavior reported to date have applied a quasi-static analysis. In this approach the dominant relaxation contribution arising from the overall tumbling of the molecule is removed from the simulation by superimposing each frame of the trajectory upon the initial frame. In the familiar case of ^{15}N amide relaxation measurements, the orientational autocorrelation for the individual $^{1}H-^{15}N$ bond vectors is then calculated as a function of time separation along the trajectory. Instead of transforming these modeled time dependent autocorrelation functions into frequency domain spectral densities to directly predict the observed T_1, T_2 and heteronuclear NOE data, "plateau" values are estimated from each bond vector autocorrelation function and compared to experimental S^2 order parameter values derived from the classical dynamical analysis of NMR relaxation data of Lipari and Szabo [1,2].

By construction, the order parameter provides a time-independent characterization of the diversity of bond vector orientations within a conformational distribution. The original Lipari–Szabo analysis, as well as the subsequent three parameter extension [3], also includes a time constant to characterize how rapidly the assumed stable conformational distribution is sampled. In practice, these derived time constants are often poorly constrained by the experimental data and are rarely used for quantitative structural interpretation [4,5]. By relating the S^2 order parameters to the spectral density values required for prediction of the NMR relaxation rates, the Lipari–Szabo formalism largely avoids the need for detailed modeling of the underlying conformational dynamics which are necessarily severely underdetermined by the available experimental data. One key assumption of this model-free approach is the independence of internal motion from the global tumbling of the macromolecule. Although factorization of the internal and global autocorrelation functions cannot be exact when the overall rotation is anisotropic [1], to a useful approximation the original assumption of isotropic tumbling can be expanded to molecular rotation according to a time-independent diffusion tensor that is either axially symmetric (4 adjustable parameters) or fully asymmetric (6 adjustable parameters) [6]. The approximation of a time-independent diffusion tensor for a conformationally dynamic macromolecule is generally believed to yield only modest errors for well-ordered single domain proteins [7], although it can more significantly fail in the presence of interdomain mobility [8].

One approach for moving beyond the assumption of independent internal and global motion is the slowly relaxing local structure approach of Freed and colleagues [9–11]. A recent implementation by Zerbetto, Buck, Meirovitch and Polimeno [12] utilized CHARMM27 [13] molecular dynamics simulations to provide estimates for the coupling potentials between global tumbling and the various sites of local motion in a two-body coupled-rotator stochastic model. The global tumbling dynamics were estimated by a hydrodynamics modeling approach. The experimental T_1, T_2 and NOE data were then used to optimize the rate of local motion and the orientation of each local frame relative to the global diffusion frame. The problem of achieving a proper Boltzmann probability distribution was resolved by postulating that the potential of mean force is adequately represented by a phenomenological equation relating the MD-derived coupling potentials and the local diffusion frames.

To adequately model global molecular tumbling in an isotropic solution, an MD trajectory needs to be long enough so that every orientation of each bond vector is approximately equally probable. Significant errors in the derived correlation function can be anticipated for trajectories that are less than 100-fold longer than the molecular tumbling time [14]. To help mitigate the effects of undersampling, Prompers and Brüschweiler [15] proposed isotropic reorientational eigenmode dynamics (iRED) covariance analysis in which the averaging over the correlated bond vector orientations within an MD trajectory is then isotropically averaged over all orientations in space. Since this analysis removes the time dependence of the bond vector correlations, correlation time information is reconstructed by projecting the reorientational eigenmodes onto the MD trajectory vectors. Analysis of a 5 ns explicit solvent simulation of ubiquitin, yielded nine largest eigenmodes with derived correlation times ranging from 368 ps to 660 ps. The top five eigenmodes were assigned to global tumbling modes, and their correlation times were then rescaled by an average factor of 7-fold to obtain values near the experimental τ_c value of 4.03 ns [16]. The correlation times of the second set of five largest eigenmodes were then rescaled by factors ranging from 1.7 to more than 4000 to achieve an optimal fit to the experimental ^{15}N relaxation data.

More recently, as microsecond long simulations have become more generally feasible, the intrinsic limitation of undersampling of molecular tumbling in simulations of modestly sized proteins has become less severe. However, an additional complication to the direct prediction of NMR relaxation values from MD simulations is that the widely used nonpolarizable water models all predict self-diffusion coefficients that are markedly higher than the experimental value. Self-diffusion for the original TIP3P model is 2.35-fold too high, while for the CHARMM-modified TIP3P model the prediction is 2.57-fold above the experimental value [17]. In this regard, the SPC model is modestly better (1.83-fold), and the SPC/E model approaches the experimental result (1.17-fold) [17]. Since for most protein backbone amide nitrogens, global tumbling provides the dominant contribution to relaxation, accurate modeling of the overall rotational diffusion is essential for robust predictions. Despite a similar issue of inaccurately modeled solvent self-diffusion, Peter, Daura and van Gunsteren [18] demonstrated that the ROESY buildup curves for various $^{1}H-^{1}H$ interactions of a heptapeptide of β-amino acids in methanol at 298 K could be reasonably reproduced from a GROMOS96 simulation. Using a 1.2 μs OPLS-AA force field simulation of ubiquitin, Shaw and colleagues [19] have extracted ^{15}N order parameters directly from the unscaled trajectory by fitting to the extended Lipari–Szabo model [3] with the molecular tumbling time optimized to 1.98 ns, reflecting the elevated self-diffusion rate of the SPC water model used in that study.

Direct prediction of experimental relaxation data offers several advantages over the more familiar comparisons with derived order parameter values. Particularly in the case of internal motion occurring on the ns timescale, there are ambiguities as to how to best extract an effective order parameter, with a resultant loss in the information content resident in the original experimental data. Full atom molecular simulations represent the current best predictions for the conformational

dynamics giving rise to the observed data. The challenge is not so much developing a model-free approach to accepting or rejecting a given force field, but rather how to assess the successes and failures within a given protein prediction. Quantifying discrepancies directly between MD modeling and experimental result will more clearly distinguish whether inadequate sampling with an accurate force field or adequate sampling with an inaccurate force field is responsible. Progress on this front will, in turn, heighten the confidence with which agreement between MD predictions and experiments can be interpreted as accurate modeling of the conformational dynamics.

The present study addresses the question of how accurately backbone ^{15}N relaxation values can be directly predicted from molecular simulations without any protein system-dependent adjustable parameterization. Primary in this consideration is whether, invoking the Stokes–Einstein equation for rotational diffusion, the known inaccuracies in the modeling of solvent self-diffusion can be used to rescale the average rotational velocity of the macromolecule so as to accurately account for its dominant contribution to ^{15}N amide relaxation behavior. The superposition between adjacent sampled frames of a trajectory yields a rotation axis and rotation angle characterizing that transition. A proportionate scaling of each such rotation angle alters the overall rotational diffusion rate without altering the relative rotational behavior with respect to the molecular frame. Thus any asymmetry in molecular tumbling predicted in the simulation will be preserved, while no recourse to a hypothetical time-independent diffusion tensor is required for representing the rotational diffusion process.

The B3 domain of Protein G provides an excellent system for testing this approach. Its elongated structure gives rise to substantial anisotropy in its rotational diffusion which, in turn, yields a marked variation in the transverse relaxation rates (R_2) among the amides in its regular secondary structure. Thus compared to more spherical proteins, prediction of an effective rotational correlation time τ_c for each residue is more problematic. This challenge is heightened by the fact that its small size (56 residues) results in a molecular tumbling rate that is near the ^{15}N Larmor frequency in high field instruments. Thus in contrast to larger proteins for which the T_1 values of the well-ordered amides increases proportionate to τ_c, the T_1 values of such residues in GB3 are less sensitive to the effective τ_c than are the T_2 values. This relaxation behavior has also contributed to GB3 and its close homolog GB1 having become the favorite system for analyzing residue-dependent variations in the amide ^{15}N chemical shift tensor by magnetic field dependent solution phase relaxation measurements [20], liquid crystal and cross-correlated relaxation measurements [21], and solid state magic-angle measurements [22,23] as well as quantum mechanics predictions [24–26]. The present analysis provides an effective basis for assessing the utility of the site-specific ^{15}N chemical shift anisotropy (CSA) values obtained by these various experimental techniques in providing NMR relaxation predictions.

2. Computational methods

2.1. Molecular dynamics simulation of the B3 domain of Protein G

Coordinates from the 1.1 Å resolution X-ray structure (PDB code 2IGD [27]) were modified with CHIMERA [28] to form the Δ1–5, T6M, T7Q variant that has been widely used for NMR studies. Hydrogen atoms were added to the protein heavy atoms and crystallographically-defined water molecules with all carboxylate and aliphatic amine groups being charged using VMD [29]. VMD was then used to form a 42.7 Å × 65.6 Å × 46.9 Å box with no protein atoms within 10 Å of the boundary. The simulation box contained 3668 TIP3P waters, as modified for CHARMM, as well as 11 sodium ions and 9 chloride ions added to establish electroneutrality and an ionic strength near 150 mM. Five parallel simulations were prepared, differing solely by independent placement of the added ions. MD simulations were carried out in NAMD2 [30] using the CHARMM27 force field [13] with Particle Mesh Ewald summation for long range electrostatics using a 1 Å grid spacing. Short range interactions utilized a switching distance of 10 Å and a cutoff of 12 Å. SHAKE constraints were applied for all bonds to hydrogen, and a step size of 1 fs was used. Steepest decent minimization was applied for 3000 steps, followed by a 30 ps warming protocol to 298 K in 25 degree increments with 5 kcal/mol/Å^2 restraints applied to all protein heavy atoms and crystallographic water molecules. Under constant temperature conditions enforced with a Langevin damping factor of 1.0 ps^{-1}, the heavy atom restraints were decreased from 5 kcal/mol/Å^2 to 1 kcal/mol/Å^2 at a rate of 10 ps per unit. The system was then allowed to stabilize under NVT conditions for 200 ps followed by another 100 ps with the heavy atom restraints reduced to 0.1 kcal/mol/Å^2. The heavy atom restraints were then removed, and 200 ns of simulation was carried out under NVE conditions with the first 5 ns being treated as equilibration. Coordinate files were stored at 5 ps intervals. Temperature drift over the trajectory was minimal with the averages over consecutive 10 ns intervals remaining within 0.1° of the overall average temperature.

2.2. Rescaling of the rotational velocity of GB3

Following translation of each trajectory frame to the all-heavy-atom center of mass, the superposition rotation between each adjacent pair of frames was determined using the quaternion algorithm described by Kearsley [31] as implemented in FORTRAN by Rupp and Parkin (PDBSUP [32]). The quaternion 4-vector describes the rotation axis vector and the magnitude of rotation that characterizes the rotational superposition. The unit-normalized quaternion is typically expressed as:

$$q = (q_0, \mathbf{q}) = (q_0, q_1, q_2, q_3) = (\cos(\theta/2), \sin(\theta/2)\boldsymbol{\nu}) \tag{1}$$

where θ is the magnitude of rotation and $\mathbf{v}$ is the axis vector for a positive rotation.

The rescaling of the rotational velocity throughout the trajectory was modeled by multiplying the angle of rotation for each step of superposition by a constant factor and then renormalizing the corresponding unit quaternion. The initial trajectory was then "rewound" by applying a rotation to each trajectory frame that is derived from a nested product of these rescaled quaternions. As illustrated for the rescaling of the Nth trajectory frame, let $(q_o, q_1, q_2, q_3)_n$ denote the rescaled unit quaternions corresponding to the superposition of consecutive trajectory frames, and let (q_w, q_x, q_y, q_z) denote the cumulative quaternion formed by nested multiplication of the $(q_o, q_1, q_2, q_3)_n$ quaternions, where n is decremented from N down to 1. For each step of the iterated quaternion multiplications [33]:

$$\begin{aligned} q_w &= q_{0n} * q_w - q_{1n} * q_x - q_{2n} * q_y - q_{3n} * q_z \\ q_x &= q_{0n} * q_x + q_{1n} * q_w + q_{2n} * q_z - q_{3n} * q_y \\ q_y &= q_{0n} * q_y - q_{1n} * q_z + q_{2n} * q_w + q_{3n} * q_x \\ q_z &= q_{0n} * q_z + q_{1n} * q_y - q_{2n} * q_x + q_{3n} * q_w \end{aligned} \tag{2}$$

For each trajectory frame the final product quaternion was then used to derive the corresponding rotation matrix [33] which was then applied to the coordinates of that frame.

$$R(\mathbf{q}) = \begin{pmatrix} 1-2q_y^2-2q_z^2 & 2q_xq_y-2q_wq_z & 2q_xq_z+2q_wq_y \\ 2q_yq_x+2q_wq_z & 1-2q_z^2-2q_x^2 & 2q_yq_z-2q_wq_x \\ 2q_zq_x-2q_wq_y & 2q_zq_y+2q_wq_x & 1-2q_x^2-2q_y^2 \end{pmatrix} \tag{3}$$

Double precision was used in the quaternion calculations with renormalization being applied following each quaternion multiplication.

2.3. $^1H-^{15}N$ bond vector autocorrelation and spectral density analysis

The lattice components of nuclear relaxation for $^1H-^{15}N$ dipolar interactions and ^{15}N CSA interactions can be expressed in terms of spherical harmonics of rank L = 2, and in an isotropic solution the bond vector autocorrelation function C(t) does not depend on the order M [1]. Hence

$$C(t) = \left\langle \frac{3(n(\tau)\cdot n(\tau+t))^2 - 1}{2} \right\rangle \tag{4}$$

where n is the unit bond vector and the trajectory time τ is incremented across the simulation. Skipping the first 5 ns of each simulation, the autocorrelation function for every backbone $^1H-^{15}N$ bond vector was calculated on each rotational velocity rescaled (RVR) trajectory. The autocorrelation functions from each of the five 200 ns simulations were then averaged.

As is well recognized, autocorrelation functions generally become increasingly unreliable at longer lag times. On the other hand, in order to obtain a robust numerical transformation of the autocorrelation function into the frequency domain, the long time tail of the autocorrelation function needs to be represented. Since global molecular tumbling quenches the time dependence of the orientational correlations for the bond vectors, an exponential extrapolation is generally presumed most appropriate. Extrapolations were carried out by performing a linear least squares fit to the logarithm of the autocorrelation function over a 0.5 ns interval and extrapolating from the middle of that interval until 50 ns. Extrapolations initiated at differing timepoints along the autocorrelation function were then transformed to spectral densities to compare the quality of the resultant NMR relaxation predictions.

The spectral densities J(ω) were calculated at the frequencies $\omega(^1H) - \omega(^{15}N)$, $\omega(^1H)$, $\omega(^1H) + \omega(^{15}N)$, $\omega(^{15}N)$ and $\omega(0)$ by summing over the autocorrelation function values [1]:

$$J(\omega) = \sum_{i=1}^{N} \frac{2}{5}(C(t_i)\cdot \cos(\omega t_i))\Delta t \tag{5}$$

where Δt was the 5 ps interval between trajectory frames. Due to the discrete nature of this transform, the term for initial timepoint was multiplied by a factor of 1.5 to represent the time interval between 0 and 7.5 ps [34]. For the optimal rotational velocity rescaling factor of 0.616, J(ω) values were calculated using trajectory frames at 10 ps and 15 ps intervals. The rms deviation for the best fit to the T_1 and T_2 values of the amides in regular secondary structure increased only slightly using the less frequent sampling. For all residues the maximum variation between the T_1, T_2 and NOE values predicted for the 10 ps sampling as compared to the 5 ps sampling was 0.5%, 0.5% and 0.007, respectively. When the analogous comparison was carried out between the 15 ps and 5 ps sampling rates, the maximal differences were 1.2%, 0.8% and 0.012, approaching the average experimental uncertainty values reported for these relaxation data [20].

2.4. Prediction of NMR relaxation parameters

The spectral densities calculated from the RVR-MD simulations were used to calculate the longitudinal and transverse relaxation rates and the heteronuclear NOE for each backbone amide $^1H-^{15}N$ bond vector [35]:

$$R_1 = \left(\frac{d^2}{4}\right)\left[J\left(\omega_{1_H} - \omega_{15_N}\right) + 3J\left(\omega_{15_N}\right) + 6J\left(\omega_{1_H} + \omega_{15_N}\right)\right] + \left(\Delta\sigma\cdot\omega_{15_N}\right)^2\left[J\left(\omega_{15_N}\right)\right] \tag{6}$$

$$R_2 = \left(\frac{d^2}{8}\right)\left[4J(0) + J\left(\omega_{1_H} - \omega_{15_N}\right) + 3J\left(\omega_{15_N}\right) + 6J\left(\omega_{1_H}\right) + 6J\left(\omega_{1_H} + \omega_{15_N}\right)\right] + \frac{\left(\Delta\sigma\cdot\omega_{15_N}\right)^2}{6}\left[4J(0) + 3J\left(\omega_{15_N}\right)\right] \tag{7}$$

$$\mathrm{NOE} = 1 + \frac{d^2}{4R_1}\cdot\frac{\gamma_{1_H}}{\gamma_{15_N}}\left[6J\left(\omega_{1_H} + \omega_{15_N}\right) - J\left(\omega_{1_H} - \omega_{15_N}\right)\right] \tag{8}$$

where $d = (\mu_o/4\pi)\hbar\gamma_{1H}\gamma_{15N}r_{HN}^{-3}$, γ is the magnetogyric ratio and Δσ is the ^{15}N CSA.

Although the major axes of the ^{15}N amide CSA tensors deviate modestly from the $^1H-^{15}N$ bond vectors, they are less accurately determined and the errors arising from not carrying out a separate autocorrelation analysis for the CSA interactions are anticipated to be small relative to the accuracy of the experimental data. Regarding the scaling of the effective bond length and CSA interactions, since the J(0) and $J(\omega_{15N})$ terms generally dominate R_1 and R_2, the ratio of the dipolar and CSA contributions to both R_1 and R_2 is approximately $3d^2/(2\Delta\sigma\cdot\omega_{15N})^2$.

3. Results and discussion

3.1. Molecular dynamics simulation of GB3

Five 200 ns NVE simulations were carried in the NAMD2 program for the B3 domain of Protein G (PDB code 2IGD) hydrated with 3668 TIP3P waters, 11 sodium ions and 9 chloride ions so that all protein atoms were at least 10 Å from an edge of the 42.7 Å × 65.6 Å × 46.9 Å box. The five parallel simulations differed only in an independent initial placement of the solvent ions and subsequent differing random seeds being used for atomic velocity assignments. The CHARMM27 force field was applied with Particle Mesh Ewald summation for long range electrostatics and SHAKE constraints for all bonds to hydrogen. An integration step size of 1 fs was used. The average temperature remained constant throughout each of the five parallel runs resulting in an overall average value of 298.4 K. To minimize systematic distortion of the prediction of conformational dynamics, pressure and temperature coupling conditions were avoided [7].

Treating the initial 5 ns as equilibration, the orientational autocorrelation function was calculated for each backbone amide $^1H-^{15}N$ vector along each trajectory and the autocorrelations were then averaged across the five simulations. As a preliminary analysis, bond vector autocorrelation functions were calculated for each amide after each frame of the trajectory had been superposed onto the initial

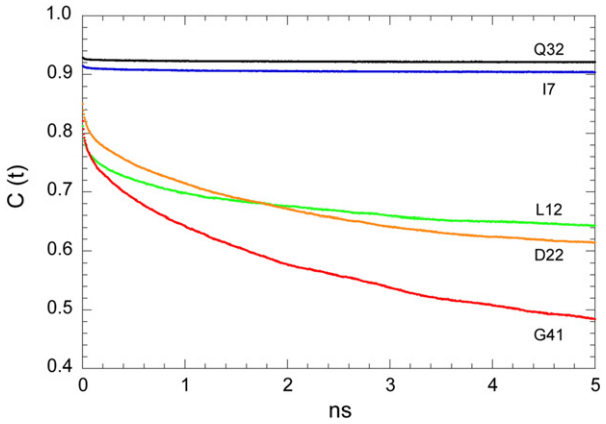

Fig. 1. $^1H-^{15}N$ bond vector autocorrelation functions for several residues of GB3 averaged over five 200 ns MD simulations with trajectory frames superimposed upon the initial frame. Leu 12 and Gly 41 exhibit the lowest experimental ^{15}N NMR order parameters in the protein, while Asp 22 presents no evidence for significant internal motion in the experimental data.

frame (Fig. 1). As is typically observed in a superpositioned trajectory for residues within regular secondary structural elements, the bond vector autocorrelation functions for Ile 7 of the first β-strand and Gln 32 of the α-helix exhibit a decrease that is largely complete by the time of the first sampling at 5 ps, followed by a plateau indicating minimal internal mobility in this timeframe.

Leu 12 and Gly 41 are reported to have the smallest ^{15}N order parameter values in GB3 [36]. In marked contrast, Asp 22 is reported to have a high order parameter consistent with little conformational mobility on the ps–ns timeframe. On the other hand, Trbovic, Kim, Friesner and Palmer [37] have reported MD simulation analysis of NMR relaxation in GB3 which predict an order parameter for Asp 22 near 0.5 using either the OPLS-AA, AMBER ff99SB or AMBER ff03 force fields. The present results indicate a qualitatively similar observation using the CHARMM27 force field for this residue. Clearly in this analysis the autocorrelation functions for Leu 12, Asp 22 and Gly 41 have not reached a plateau value in the timeframe of molecular tumbling (3.3 ns [36]).

When bond vector autocorrelation analysis is applied directly to the trajectory coordinates and then displayed on a semi-log plot, several distinct observations are apparent (Fig. 2). In contrast to Fig. 1, the difference between residues Ile 7 and Gln 32 is far more evident than that between residues Leu 12 and Gly 41. The $^{1}H-^{15}N$ bond vector of Gln 32 lies along the α-helical axis which is, in turn, nearly collinear with the major axis of the diffusion tensor [36]. The amide bond vector of Ile 7 is approximately perpendicular to the major axis. These relative differences illustrate the dominant role of molecular tumbling in the overall relaxation behavior and hence the critical requirement for accurately modeling the global motion in order to accurately characterize internal motion, particularly those occurring on a similar timeframe.

In the neighborhood of 2 ns, the ln C(t) curves for Ile 7 and Gln 32 begin to deviate from simple linearity. Particularly relevant is the fact that they both become concave beyond this point. If there were slower components of motion that become increasingly significant at these longer correlation times, due either to non-exponentiality in global tumbling or slower internal motions, the curvature of the log autocorrelation function would become convex. The concavity in the Ile 7 and Gln 32 log autocorrelation curves is presumably a manifestation of inadequate statistical sampling at these longer correlation times. Similarly, at timepoints beyond 2.5 ns, the log autocorrelation curves for Leu 12 and Gly 41 exhibit anomalous curvatures suggestive of inadequate statistical sampling.

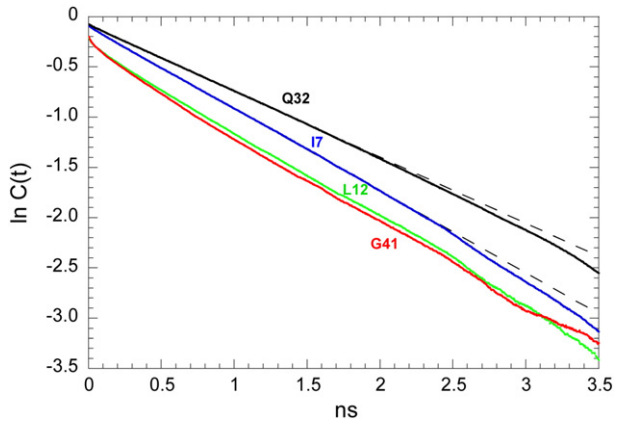

Fig. 2. $^{1}H-^{15}N$ bond vector autocorrelation functions for several residues of GB3 averaged over five 200 ns MD simulations for the original trajectory displayed as a semi-log plot. Despite the absence of significant internal motion on the ps–ns timescale, Ile 7 and Gln 32 differ markedly in the decay of their bond vector autocorrelation functions as a result of their relative orientation with respect to the major axis of rotational anisotropy.

3.2. Rescaling of rotational velocity

The $^{1}H-^{15}N$ bond vector autocorrelation functions of Ile 7 and Gln 32 from the original trajectory drop to e^{-1} in 1.2 and 1.4 ns, respectively, indicating an effective molecular correlation time that is ~2.5 times smaller than the experimental value. As noted above, self-diffusion for the CHARMM-modified TIP3P water model is 2.57-fold above the experimental value [17]. The similarity of these values suggests that if the molecular tumbling process were analogously scaled, the resultant trajectory might provide an effective model for the contribution to NMR relaxation arising from the global motion. To examine that possibility, we carried out a rescaling of the effective rotational velocity of the five 200 ns simulations.

The global change in orientation between adjacent frames from a trajectory can be represented by the rotation relating the superpositioning of all heavy atoms for those two frames. The 4-vector quaternion representation specifying both the unique axis of rotation and the magnitude of rotation about that axis provides the most efficient means of expressing the concatenation of a series of rotations. The step size of the transition relating the adjacent frames can thus be simply scaled by adjusting the magnitude of the rotation. In order to apply this rotational rescaling consistent with the non-commutativity of rotations, the frames from the original trajectory must be shifted to their center of mass and then "rewound". For the final frame, the quaternion specifying rotation to transform it back toward the previous frame is determined. It is then multiplied by the quaternion that specifies the scaled transformation relating the two previous frames. This nested product of quaternions is then continued until the initial frame of the trajectory is reached. The resultant product quaternion for the final frame is then transformed into a rotation matrix which is applied to the coordinates of the original final frame. All other frames are transformed analogously.

A measure of the robustness of this rotational rescaling protocol can be obtained by comparing the fully rewound trajectory with the conventional superpositioning of all frames onto the initial frame. Since, in general, no global superpositioning can satisfy all pairwise superpositioning optima [33], these two approaches cannot be expected to provide identical results. Furthermore, with an effective molecular correlation time of ~1.3 ns, during a 200 ns simulation the GB3 molecule will have rotationally diffused through one radian approximately 150 times, and a series of up to 40,000 concatenated rotations are required to rewind the simulation. Nevertheless, the all heavy atom rms deviation between the coordinates for all 40,000 frames of the fully rewound trajectory and the coordinates of these frames superimposed upon the first frame is only 0.59 Å, when averaged over the five trajectories. More directly germane to the relaxation analysis, the rmsd for the difference in orientation of the corresponding backbone N–H bond vectors varies from 1.5° to 4.0° among the five 200 ns simulations, with a mean value of 3.15°. For comparison, it may be noted that an S^2 value of 0.85 corresponds to a semi-angle of 19° for the diffusion-in-a-cone model. Since the differences in bond vector orientation in the fully rewound original trajectory as compared to the original trajectory superimposed upon the initial frame would surely be statistically independent of any internal motion, their contribution to the predicted order parameters could enter at most as the sum of the variances (i.e. a semi-angle of 19.2° vs 19.0°).

3.3. Predicting the optimal molecular rotational rescaling for GB3

Brownian rotational motion is standardly modeled as a Weiner process which implies that a doubling of the step size will increase the rotational diffusion rate 4-fold. Thus the 2.57-fold elevation in the self-diffusion rate of CHARMM-modified TIP3P water, relative to experiment, would imply the need to reduce the effective rotational velocity by 1.6-fold. For any given rotational rescaling factor, the bond vector autocorrelation function for each backbone amide is

calculated from the rotationally rescaled trajectory. The autocorrelation functions are then transformed into frequency space to yield the spectral density functions used to predict the NMR relaxation rates. As discussed above, the statistical sampling of the autocorrelation functions derived from these MD simulations of GB3 appears to become unreliable for lag times longer than a few ns. On the other hand, a robust numerical transformation of the autocorrelation function into the corresponding spectral density function requires a representation of the long time tail of the autocorrelation function. As expected from the dominant contribution of molecular tumbling to the decay of the autocorrelation function, the calculations of Fig. 2 clearly support the use of exponential extrapolation for modeling the long lag times. Since it is desirable to use as much of the calculated autocorrelation data as practical, the timepoint beyond which an extrapolated tail to the function is utilized is treated as a system-wide optimizable variable. Since this need to extrapolate the autocorrelation function is a result of inadequate sampling, the appropriate timepoint for exponential extrapolation should, in principle, simply depend upon the length of the trajectory.

As is apparent from Eq. (5), the zero frequency component of the spectral density function J(0) is proportional to the integral of the autocorrelation function which, in turn, is standardly considered the effective correlation time for that bond vector orientation. In Fig. 3 is displayed the J(0) values for the backbone amide H–N bond vectors of GB3 calculated from the original unscaled NVE simulations. The variations in the J(0) values from the unscaled simulations are fairly modest with an evident region of elevated values between Ala 23 and Asp 36. A similar elevation in the R_2 values of these residues of the long α helix was noted during analysis of the experimental relaxation measurements, consistent with an enhanced relaxation rate due to the alignment of the helical axis along the major diffusion axis of the protein [36]. When the original GB3 trajectories were rescaled to a rotational velocity consistent with the experimental diffusion rate of water, the corresponding J(0) values generally increase by approximately 2.5-fold (Fig. 3). An increased variability in the J(0) values is apparent in the rescaled trajectories as seen for the residues Asp 22 and Gly 41, discussed previously, as well as for several residues in the loop between the first and second strands of the β sheet. In addition, a sawtooth pattern is observed for the J(0) values in the α helix as previously noted in both experimental [36] and simulation [7] studies of GB3 relaxation. The residue-specific variabilities in the predicted J(0) are less apparent in the unscaled trajectories due, in part, to the fact that the accelerated global tumbling in the original simulation more completely dominates the relaxation contribution that arises from the smaller scale internal motion.

Having derived a spectral density function from the rotational velocity rescaled MD simulations, two other imprecisely determined

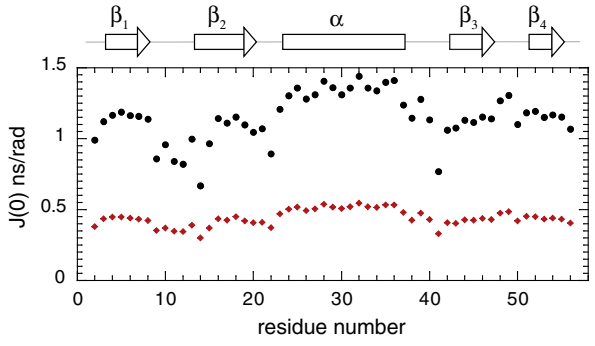

Fig. 3. Zero frequency spectral density function J(0) calculated for the rotational velocity rescaled GB3 trajectories using a rescaling factor of 0.616 and a timepoint for exponential extrapolation of 2.5 ns (circles). The analogous J(0) values obtained by applying this timepoint to the original unscaled trajectories are indicated as red diamonds.

parameters must be specified in order to calculate the longitudinal and transverse relaxation rates R_1 and R_2, the effective $^1H-^{15}N$ bond length and the ^{15}N chemical shift anisotropy(ies). When viewed in terms of optimizing parameters to match experimental R_1 and R_2 values, for moderate sized proteins an increase in the estimated molecular correlation time increases R_2 and decreases R_1 nearly proportionately. In contrast, an increase in the effective $^1H-^{15}N$ bond length decreases the dipolar contribution to both R_1 and R_2 relaxation by the same proportion. Similarly, decreasing the ^{15}N CSA value yields a proportionate decrease in that contribution to both R_1 and R_2 relaxation. Not only do the CSA contributions to R_1 and R_2 depend solely on the spectral densities $J(\omega_{15N})$ and $4J(0)+3J(\omega_{15N})$, respectively, these same spectral density components dominate the dipolar R_1 and R_2 relaxation in macromolecules as well. As a result, the ratio of the dipolar and CSA contributions to both R_1 and R_2 is approximately $3d^2/(2\Delta\sigma\cdot\omega_{15N})^2$, predicting a 2.6-fold larger dipolar contribution at a magnetic field of 14.1 T. Thus for 600 MHz data, the relaxation effect of increasing the $^1H-^{15}N$ bond length by 0.004 Å is essentially indistinguishable from the effect of a 5 ppm decrease in the CSA value.

The majority of protein NMR relaxation studies have utilized a $^1H-^{15}N$ bond length of 1.02 Å which, when combined with a ^{15}N chemical shift anisotropy value of 160 ppm, typically yields derived S^2 values near 0.85 for the residues in regular secondary structures. As discussed by Case [38], it is useful to regard an order parameter as a ratio relating the observed dipolar coupling strength to that which would be expected from some reference situation. The standard $^1H-^{15}N$ bond length value of 1.02 Å can be understood as modeling a hypothetically rigid dipole separation with no motional averaging. For interpreting the thermally activated motions modeled by classical MD simulations, an effective average dipole bond length must incorporate both quantum mechanical zero-point motion and any attenuated classical bond fluctuations as might arise when the bonds to hydrogen atoms are rigidified by the SHAKE [39] algorithm. The theoretical analysis of Case led to an optimal effective ^1H-^{15}N bond length value of 1.04 Å, which agreed quite well with the previously reported estimate of Ottiger and Bax [40] derived from their analysis of residual dipolar coupling data as well as subsequent dipole–dipole cross correlated relaxation rate measurements [41]. To compare the plateau levels predicted in the autocorrelation functions derived from MD simulations to experimentally derived S^2 order parameters, the plateau levels are often multiplied by $(1.02/1.04)^6 \sim 0.89$, although as discussed below, a somewhat higher normalization value may be more appropriate.

Although differences in hydrogen bonding patterns may give rise to small residue-specific variations in the effective $^1H-^{15}N$ bond length [38,42,43], considerably more attention has been given to analyzing the degree to which structural variations give rise to significant residue-specific variations in the ^{15}N CSA values. GB3 and its close homolog GB1 have played a central role in the efforts to determine amide ^{15}N chemical shift tensors by solution phase relaxation, liquid crystal and cross-correlated relaxation, and solid state magic-angle measurements as well as quantum mechanics predictions [24–26]. The magnetic field dependent ^{15}N relaxation measurements of Hall and Fushman [20] deduced a range of residue-specific CSA values from 111.3 to 240.8 ppm for GB3. The liquid crystal and cross-correlated relaxation measurements of Bax and colleagues [21] yielded a smaller range of 148 to 187 ppm, while the CSA values derived from solid state magic-angle measurements by Rienstra and colleagues [22,23] span a 50 ppm range, half of that range arising from an anomalously small value for the mobile Gly 41 residue. To assess the degree to which these residue-specific CSA values might enhance the ability to predict ^{15}N relaxation data, we have also included in our analysis additional calculations based on a uniform CSA value.

To derive the best fit to the experimental relaxation data from rotational velocity rescaling of the MD simulation, a total of four variables must be optimized — the rescaling factor, the timepoint for exponential

extrapolation and the operationally correlated variables of the effective $^{1}H-^{15}N$ bond length and ^{15}N CSA value. At a given magnetic field, specifying the CSA value(s) will yield a corresponding optimal bond length. The robustness of a given set of CSA values can then be tested by carrying out the analogous analysis as a function of magnetic field to see whether a field-independent bond length is predicted.

T_1 and T_2 data from 32 amides of GB3 that lie within the α-helix or the four β-strands were used to optimize the molecular rotational rescaling. For a constant CSA value of 168 ppm, the minimum rmsd fit to the experimental R_1 and R_2 values [20] at 14.1 T (600 MHz ^{1}H) was determined as a function of the rescaling factor and the timepoint for exponential extrapolation (Fig. 4A). The overall minimum rms deviation from the experimental R_1 and R_2 values of 2.2% was obtained when the 0.5 ns interval of autocorrelation function data used to generate the exponential extrapolation to long lag times starts at 2.5 ns. This minimum occurs when the rotational velocity rescaling (RVR) factor is 0.616 which corresponds quite well with the value of 0.624 predicted from the self-diffusion calculations for CHARMM-modified TIP3P water. The optimal $^{1}H-^{15}N$ bond length is largely insensitive to the choice of rescaling factor and timepoint for exponential extrapolation and is 1.039 Å for the optimization with a CSA value of 168 ppm. A virtually indistinguishable plot is obtained with the more commonly invoked CSA value of 160 ppm which yields an optimal $^{1}H-^{15}N$ bond length of 1.033 Å.

As might be anticipated from the near linearity of the log autocorrelation plots illustrated in Fig. 2, the quality of the optimal percent deviation is not markedly worse when the exponential extrapolation is applied at an earlier timepoint in the autocorrelation function. On the other hand, the quality of the fit rapidly degrades when the exponential extrapolation is applied at later timepoints in the autocorrelation function, consistent with the onset of significantly poorer sampling statistics.

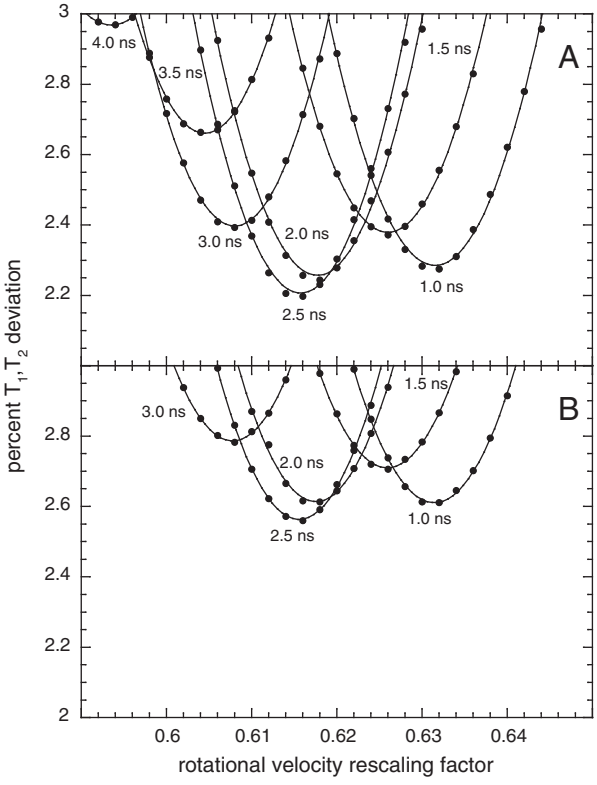

Fig. 4. Prediction of ^{15}N T_1 and T_2 values at 600 MHz for 32 residues in the regular secondary structures of GB3 as a function of the velocity rescaling factor applied to each step of rotation in the trajectory. In panel A are illustrated the optimal predictions with the ^{15}N CSA values set to 168 ppm as a function of the effective $^{1}H-^{15}N$ bond length when the 0.5 ns interval used to derive an exponential extrapolation for the bond vector autocorrelation function is initiated at 1.0 ns, 1.5 ns, 2.0 ns, 2.5 ns , 3.0 ns, 3.5 ns or 4.0 ns. The rescaling factor dependence of the percent deviations closely follows a quadratic form. In panel B are illustrated the analogous results when the solid state NMR estimates of the residue-specific ^{15}N CSA values [22] are used.

Hall and Fushman [20] report that the average experimental uncertainty in the R_1 values at 14.1 T for these 32 residues of GB3 is 1.65%, while the corresponding average estimated error in the R_2 measurements is 1.59%. The RVR-MD analysis presented in this paper directly predicts these experimental values to nearly within the estimated experimental error using only a rotational velocity rescaling factor that closely corresponds to the earlier solvent self-diffusion calculations [17], the independently established $^{1}H-^{15}N$ bond length of 1.040 Å [38,40,41], and an average CSA value of 168 ppm, which closely matches a recent experimental estimate of 169 ppm derived from the field dependence of the NMR relaxation of ubiquitin [44].

Rienstra and colleagues [22] have reported solid state NMR measurements of ^{15}N CSA tensor values for the closely homologous GB1, including 21 of the 32 amides in regular secondary structure used in the optimization of rotational velocity rescaling. To facilitate comparison, the CSA values for the other 11 amides were set to the average value for the 21 reported residues (164 ppm) with the result that at the optimal fitted ^{1}H-^{15}N bond length (1.036 Å), the T_1 and T_2 predictions for those 10 residues closely match those of the uniform CSA analysis above. Thus the difference in percent T_1, T_2 deviations predicted from the solid state NMR measurements (Fig. 4B) as compared to the predictions from the uniform CSA assumption (Fig. 4A) arise only from the differing predictions for the 21 residues with experimental CSA data. The pattern of percent deviations in the T_1 and T_2 predictions using the solid state NMR residue-specific CSA values is qualitatively similar to that for the uniform CSA analysis, although the rms deviations are increased by nearly 0.4%.

When an analogous comparison was carried out using residue-specific CSA values derived from liquid crystal and cross-correlated relaxation measurements by Yao, Grishaev, Cornilescu and Bax [21] a similar pattern of percent T_1, T_2 deviations was obtained with the minimum occurring at the same rotational velocity rescaling factor of 0.616 and an exponential extrapolation interval beginning at 2.5 ns. However, in this case the optimal rms deviation is 3.0%. The NMR relaxation data used in the present analysis were reported by Hall and Fushman [20] in their study of the magnetic field dependence of ^{15}N relaxation as a means to estimating residue-specific CSA values. When their CSA values are incorporated into the RVR-MD based predictions of their own T_1 and T_2 data, the minimum rms deviation is 6.8%. At this minimum, the rotational velocity rescaling factor is shifted to 0.620, the exponential extrapolation interval begins at 2.0 ns, and the optimal $^{1}H-^{15}N$ bond length is 1.043 Å. The minimum rms deviation for predictions based on the residue-specific CSA values of Hall and Fushman decreases to 5.0% if Phe 52 is removed.

The ability to predict the individual transverse relaxation rates for these 32 amides of the regular secondary structure for these four different approaches to modeling the CSA interactions is illustrated in Fig. 5. The range in experimental R_2 values from 4.5 to 6.0 s^{-1} reflects the marked variations in effective tumbling rates for the individual $^{1}H-^{15}N$ bond vectors that differ in their orientation with respect to the asymmetric molecular diffusion, as reflected in the J(0) values of Fig. 3. The excellent agreement achieved by the analysis utilizing a constant CSA value demonstrates that, despite the inaccuracy in the predicted rate of rotational diffusion in the TIP3P solvent, the asymmetry of that tumbling is correctly predicted and is faithfully preserved during the rescaling of the rotational velocity (Fig. 5A). The modestly increased errors in R_2 predictions derived from the CSA values obtained by solid state NMR (Fig. 5B) and the liquid crystal and cross-correlated relaxation measurements (Fig. 5C) are generally dispersed throughout the protein sequence. Although substantially larger errors in R_2 predictions from the magnetic field dependence-based estimates of residue-specific CSA values were evident

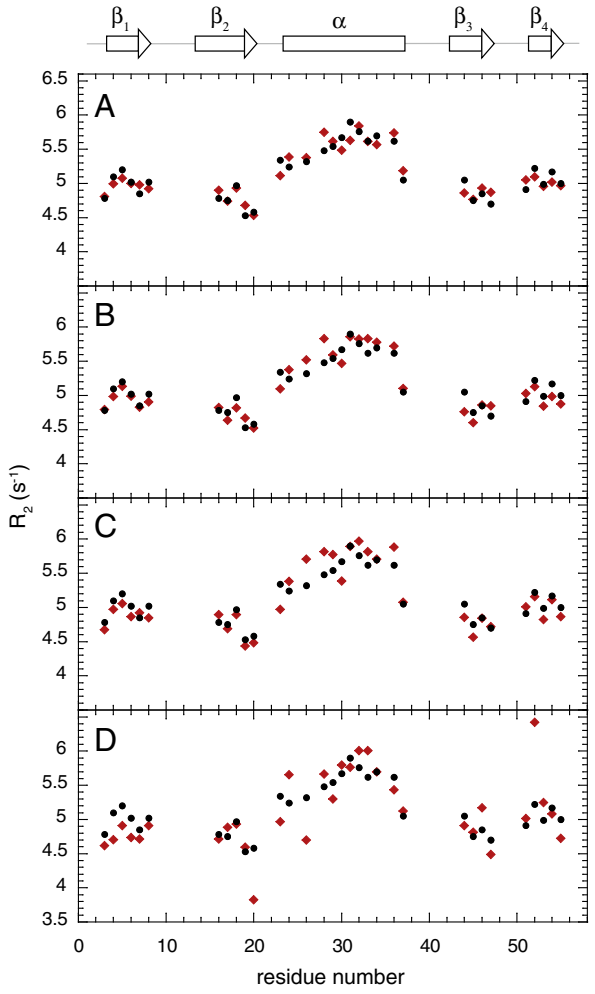

Fig. 5. Prediction of ^{15}N transverse relaxation rates at 600 MHz for 32 residues in the regular secondary structures of GB3 as a function of ^{15}N CSA parameterization. The experimental values [20] are indicated as circles, the RVR-MD predicted values are indicated as red diamonds. Results are given using a constant CSA value of 168 ppm (panel A) and residue-specific CSA values derived from solid state [22] (panel B), liquid crystals [21] (panel C) and isotropic solution [20] (panel D). The optimal $^{1}H-^{15}N$ bond length used for each calculation is given in Table 1.

throughout the sequence (Fig. 5D), markedly larger discrepancies were obtained at Ala 20 (CSA = 128.1 ppm), Ala 26 (CSA = 136.0 ppm) and Phe 52 (CSA = 240.8 ppm).

At a given magnetic field this RVR-MD based analysis cannot independently identify the optimal values for the $^{1}H-^{15}N$ bond length and the average ^{15}N CSA value. However, for a series of magnetic fields, a globally optimal average CSA value could be expected to predict a field-independent optimal bond length. As illustrated in Table 1, for an assumed average CSA value of 160 ppm, the optimal $^{1}H-^{15}N$ bond length varies from 1.037 Å at 9.4 T to 1.031 Å at 18.8 T. In contrast, using an average CSA value of 168 ppm, the optimal $^{1}H-^{15}N$ bond length is more uniform with an average optimal $^{1}H-^{15}N$ bond length of 1.040 Å over the well-predicted lower three magnetic fields. When the corresponding analysis is carried out using the residue-specific CSA values of Hall and Fushman, with an average CSA of 173 ppm for these 32 residues, the correlation between magnetic field strength and optimal $^{1}H-^{15}N$ bond length is the reverse of that observed for the uniform 160 ppm CSA analysis. In contrast, the residue-specific CSA values derived from liquid crystal and from solid state measurements, with average CSA values of 167 and 164 ppm respectively, exhibit little magnetic field dependence in their predicted optimal $^{1}H-^{15}N$ bond lengths. At all fields the rms deviation for the relaxation predictions increases in going from the uniform CSA assumption to the solid state-derived and then to the liquid crystal-derived CSA values.

Inaccuracies in the measurement of the residue-specific CSA values by either liquid crystal or solid state NMR measurements might account for resultant ^{15}N relaxation predictions being less robust than those for a constant CSA value. As indicated in Fig. 5, the increased errors from these residue-specific CSA based relaxation predictions are well distributed throughout the sequence, rather than arising from a few aberrant positions. Furthermore, indication of a significant information content in these residue-specific CSA values comes from the correlation coefficient of 0.80 between the liquid crystal and solid state NMR measurements for these 32 residues (correlation of ^{15}N CSA values from liquid crystal and solid state NMR measurements — Fig. S1 — Supplemental materials), despite the markedly different experimental approaches used in these two studies.

If the reported residue-specific CSA values are statistically significant, then the poorer predictive performance obtained using these values implies an additional source for error in the RVR-MD based relaxation analysis. The rotational velocity rescaling factor and the timepoint for exponential extrapolation are unlikely to provide a source for such compensating errors due to their global character and the fact that optimization of these two parameters is very weakly coupled to variations in either the assumed CSA value or $^{1}H-^{15}N$ bond length. On the other hand, both ^{15}N CSA values [24–26] and $^{1}H-^{15}N$ bond lengths [38,42,43] are known to be sensitive to changes in hydrogen bond interactions. In particular, Tang and Case [26] have recently presented QM/MM calculations indicating the ^{15}N CSA value for specific peptide units in GB3 tend to increase in the order of no hydrogen bonding, hydrogen bonding to the N–H only, hydrogen bonding to C═O only, and hydrogen bonding at both the N–H and C═O. The increments of these changes in CSA values are on the order of 5 ppm. Previously, Case [38] reported MP2 calculations indicating that formation of a hydrogen bond to water lengthens the H–N bond of N-methylacetamide by about 0.004 Å.

These various calculations suggest that the relative magnitude of the concerted increases in H–N bond length and ^{15}N CSA value induced by hydrogen bond formation lead to a substantial mutual cancellation of their individual contributions to the ^{15}N relaxation processes. As a result, when a relaxation analysis combines residue-

Table 1
Magnetic field dependence of ^{15}N T_1 and T_2 predictions for 31 well-ordered residues of GB3.[a,b,c].

		400		500		600		700		800	
	CSA_{ave}	r_{NH}	%rmsd	r_{NH}	%rmsd	r_{NH}	%rmsd	r_{NH}	%rmsd	r_{NH}	%rmsd
Uniform	160	1.037	1.84	1.036	2.61	1.033	2.21	1.034	4.16	1.031	5.47
Uniform	168	1.040	1.83	1.041	2.61	1.039	2.21	1.042	4.16	1.042	5.47
SSNMR [22]	164	1.039	2.08	1.038	2.99	1.036	2.59	1.038	4.83	1.037	6.19
RDC [21]	167	1.040	2.36	1.040	3.59	1.038	3.00	1.041	5.75	1.041	7.19
B field [20]	173	1.041	3.03	1.043	3.74	1.043	5.04	1.048	4.49	1.050	4.77

[a] Of the amides in regular secondary structure, Phe 52 is not included.
[b] Rotational velocity rescaling factor of 0.616, except for B field uses 0.620.
[c] 2.5 ns lag time for exponential extrapolation, except for B field uses 2.0 ns.

specific CSA values with the assumption of a uniform H – N bond length, the errors will be enhanced. Given the ability to predict relaxation values to nearly within experimental uncertainty using uniform average values for the $^{1}H-^{15}N$ bond lengths and ^{15}N CSA, residue-specific values for these parameters are unlikely to offer significant improvement. Combined with previous independent estimates of the effective $^{1}H-^{15}N$ bond length [38,40,41], the fact that an average CSA value of 168 ppm yielded optimal effective $^{1}H-^{15}N$ bond lengths near 1.040 Å at each magnetic field provides additional credibility to the robustness of this joint optimization. However, it should be noted that the reliability of this pair of optimal parameters depends not only on the accuracy of the reported average magnetic field dependence of the changes in GB3 relaxation parameters but also on the absolute accuracy of those relaxation measurements.

Predicted S^2 values scale with the assumed average $^{1}H-^{15}N$ bond length. Based on analysis of dipolar couplings, Yao, Vögeli, Ying and Bax [42] recently proposed an equilibrium bond length of 1.023 Å that closely matches neutron diffraction measurements [45]. When combined with an average ^{15}N CSA value of 168 ppm, the predicted S^2 values would decrease 1.3% relative to those predicted using a bond length of 1.020 Å and an average ^{15}N CSA value of 160 ppm. These parameters imply that MD-derived autocorrelation plateau values would be more appropriately scaled by 0.932 when comparing to experimentally derived ^{15}N order parameter values, taking into account both the bond length scaling $(1.023/1.040)^6$ and the proportion of ^{15}N relaxation arising from the dipolar interaction (~0.72 at 600 MHz).

3.4. Prediction of ^{15}N relaxation parameters for GB3

The experimental heteronuclear NOE data was not used in the derivation of the optimal rotational velocity rescaling for GB3. When NOE values at 600 MHz are predicted for the 32 residues used in this optimization, the predicted values are systematically higher, on average, than the reported NOE values by 0.026. If the mean of the predicted NOE values is shifted accordingly, the rms deviation between the predicted and observed values is only 0.018, comparable to the estimated experimental uncertainty [20]. NOE measurements are notoriously sensitive to systematic bias. In particular, one may note a recent series of papers by Ferrage, Cowburn, Ghose and colleagues [46–48] analyzing the effects of the saturation scheme and water suppression techniques in quantifying protein ^{15}N NOE signals. They demonstrate that versions of the heteronuclear NOE experiment in common use can give rise to differences of 0.1. Inaccuracies in the NOE measurements predominantly impact the estimated timescale of rapid internal motion which are generally recognized to have limited reliability. In contrast, errors on the order of 10% in the NOE generally lead to errors in the derived S^2 order parameters of only 1% [47]. An obvious potential benefit of direct MD-based prediction of NMR relaxation parameters would be to further stimulate the development and general implementation of more accurate heteronuclear NOE measurements.

When the RVR-MD analysis is considered for the other 23 backbone amides of GB3, the relaxation parameters for many of these residues are also well-predicted (Fig. 6). Only two residues of GB3 exhibit experimental ^{15}N S^2 order parameters below ~0.7, Leu 12 (~0.6) and Gly 41 (~0.5) [36]. The R_2 values for both of these residues are exceptionally well-predicted. For Gly 41 the experimental R_1 and NOE values are both lower than predicted, suggesting that some relatively rapid internal motion of significant amplitude is not being adequately modeled. The dominant contribution to relaxation arising from global tumbling is illustrated by applying the same CSA, bond length and exponential extrapolation timepoint values to the original unscaled trajectory (R_1, R_2 and NOE predicted from unscaled trajectory — Fig. S2 — Supplemental materials). Since in this case the effective global correlation of ~1.3 ns is on the fast limit side of the ^{15}N Larmor frequency, the R_1 values are modestly underestimated, the R_2 values generally decrease

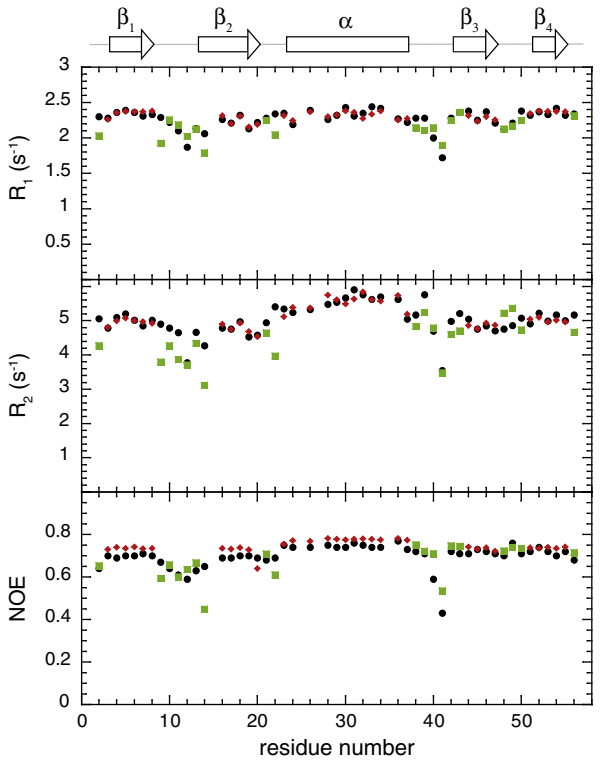

Fig. 6. Prediction of ^{15}N R_1, R_2 and NOE values at 600 MHz for GB3 using a rotational velocity rescaling factor of 0.616 applied to each step of rotation in the trajectory, 168 ppm for all ^{15}N CSA values, and an effective $^{1}H-^{15}N$ bond length of 1.039 Å. The experimental values [20] are indicated as circles. The RVR-MD predicted values for the 32 residues of the regular secondary structures are indicated as red diamonds, while the predictions for all other residues are indicated as green squares.

proportionate to the change in global correlation time, and the NOE values decrease toward zero as the characteristic frequency for the null of that function is approached.

There are two internal positions for which the full RVR-MD analysis predicts substantial internal motion that is not apparent in the experimental relaxation data, Asp 22 and the loop contacting the β_1 and β_2 strands (Fig. 6). Similar to these CHARMM27 force field calculations, Trbovic, Kim, Friesner and Palmer [37] have reported low S^2 values for these same two positions using each of the OPLS-AA, AMBER ff99SB and AMBER ff03 force fields. For the case of Asp 22, they identify in their molecular simulations a transient flip of the preceding peptide bond that enables the carbonyl oxygen of Val 21 to form a hydrogen bond to the phenolic hydroxyl of Tyr 3 that is not seen in the crystal structure. In the second region a larger scale effect is seen involving changes in the dynamics for all of the residues between Gly 9 and Gly 14. These authors proposed that at least part of this increase in predicted conformational dynamics involves a flip of the peptide group linking Asn 8 and Gly 9. As a result, the amide nitrogen of Gly 9 exchanges the hydrogen bond with the carbonyl oxygen of Leu 12, as seen in the X-ray structure, for a non-native hydrogen bond to the sidechain carbonyl oxygen of Asn 8.

Analysis of the geometric distribution of conformations at the sites in GB3 that gave rise to aberrant NMR relaxation predictions from OPLS-AA, AMBER ff99sb and AMBER ff03 calculations led Trbovic, Kim, Friesner and Palmer [37] to propose a common source of inaccuracies in the relative balance between hydrogen bonding and other terms in all three force fields. Our results with CHARMM27-based GB3 NMR relaxation and, more generally, the elevated rotational diffusion predictions of the common non-polarizable water models

provide further support for the interpretation that incorporation of explicit polarization effects may prove critical to the accurate modeling of hydrogen bonding interactions.

3.5. Utility of direct prediction of NMR relaxation parameters for assessing force field accuracy

If quantitative prediction of NMR relaxation is to provide an effective approach for assessing the accuracy of a given force field, it is crucial to establish a basis for interpreting differences between the predicted and observed relaxation values. The more robustly such an interpretation can be rendered, the increased confidence researchers will have to interpret an agreement between prediction and observation as reflecting an accurate modeling of the conformational dynamics. As illustration, this rotational velocity rescaled modeling of GB3 dynamics has yielded a highly precise prediction of the R_2 value for the mobile residue Leu 12 (Fig. 6). However, given the markedly inaccurate R_2 predictions for the residues on either side of this position, it is hard to avoid the suspicion that the agreement for the Leu 12 amide may be coincidental.

Fundamental to any quantitative interpretation of MD-based predictions of protein NMR relaxation is the assumption that the trajectory lies within a highly populated region of the native state conformational distribution so that predictions based on that trajectory can have a statistically significant contribution to the experimentally observed values. The straightforward interpretation of deviations between the predicted and observed relaxation values is that if the predictions indicate significantly less motion in the ps–ns timeframe than indicated by the experimental data, then either there is insufficient conformational sampling or the force field is too rigid or energetically skewed toward the starting state. If, instead, substantially more motion at a given site is predicted, insufficient conformational sampling becomes a less plausible explanation since the unsampled regions of the native state conformational distribution must not only have reduced dynamics in that site, but the population of these less mobile conformations must dilute away the statistical impact of the conformations sampled in the trajectory. Alternatively, prediction of substantially more motion at a given site indicates that the force field is either too fluid or energetically skewed toward other conformational states. RVR-MD analysis provides a basis for assessing these interpretations in more detail.

Contrary to the MD-based predictions given here as well as the earlier MD results of Trbovic, Kim, Friesner and Palmer [37], the experimental NMR relaxation data for Asp 22 do not appear consistent with substantial internal motion in the ps–ns timeframe. To examine this issue in more detail, we invoke the assumption of statistical independence between rapid sub-ps motion ($C_f(t)$), the slower ps–ns internal motion that gives rise to decreasing autocorrelation functions for the superimposed trajectory frames ($C_s(t)$), and the global tumbling ($C_M(t)$). It should be emphasized that no such assumption of statistical separability has been invoked in the RVR-MD analysis presented earlier in this manuscript. Under the separability assumption, the autocorrelation function contribution arising strictly from global tumbling can be obtained by dividing the corresponding autocorrelation function for the rotational velocity rescaled trajectory by the autocorrelation function for the fully rewound trajectory ($C_M(t) = C_{RVR}(t)/C_{rew}(t)$). Separability implies that the autocorrelation function for the fully rewound trajectory $C_{rew}(t) = C_f(t) \cdot C_s(t)$. Further deconvolution requires an independent estimate of the plateau level that characterizes the fast internal motion autocorrelation function $C_f(t)$.

In the case of Asp 22, the experimental relaxation values appear qualitatively consistent with negligible slower scale ps–ns internal motion (i.e., $C_s(t)$). By multiplying the global tumbling contribution to the autocorrelation function $C_M(t)$ by a generic plateau autocorrelation function $C_f(t)$, as illustrated for Ile 7 and Gln 32 in Fig. 1, the corresponding spectral densities can be derived. Scaling the level of the plateau in that generic $C_f(t)$ to 0.920 resulted in spectral densities that predicted the ^{15}N T_1, T_2 and NOE values for Asp 22 to within 2%, comparable to the accuracy that was obtained for the RVR-MD analysis of the 32 residues in the regular secondary structures of GB3. Multiplying this plateau level of 0.920 by the factor of 0.932 that we propose for the scaling between MD predictions and experimental order parameters yields a predicted S^2 value of 0.86 which agrees very closely with that reported experimental value for Asp 22 [36]. Given a reasonable representation for the fast internal motion autocorrelation function for Asp 22, the slow internal motion autocorrelation function can be derived as $C_s(t) = C_{rew}(t)/C_f(t)$. As anticipated from autocorrelation function for this residue when each trajectory is superpositioned onto the initial frame (Fig. 1), the derived $C_s(t)$ is poorly represented by a single exponential, indicating potential limitations of more simplified analyses that invoke a similar assumption of separability.

As argued by Trbovic, Kim, Friesner and Palmer [37], the disparity between the predicted and observed relaxation behavior of Asp22 (as well as for the loop surrounding Leu 12) is most plausibly interpreted as indicating either a marked overestimation of the relative population of the non-crystallographic conformations at these sites or else that the rate of conformational interchange at these sites has been significantly overestimated by the MD simulations. These two alternatives can be directly examined by scaling the predicted autocorrelation function for the slower ps–ns internal motion $C_s(t)$, either by reducing the amplitude of this component so as to model a reduced population of the non-crystallographic conformation or by the stretching of the time axis for $C_s(t)$ to model a slower rate of conformational interchange. As indicated in Fig. 1, the value of the autocorrelation function for Asp 22 at the first timepoint sampled is 0.85 for either the superimposed or fully rewound trajectories. Even if all of the timepoints above 5 ps were stretched to infinity on the timescale, using a plateau value of 0.85 to model the internal motion of Asp 22 yields R_1 and R_2 predictions that underestimate the experimental values by 6.3% and 10.4%, respectively. This disparity suggests that a force field error solely in the rate of conformational interchange would have to be at least on the order of 10^3 or more.

It would seem more likely that an overestimate of the relative population of the non-crystallographic conformation is also occurring. To assess this possibility, spectral densities were calculated in which a differing proportion of the derived Cs(t) autocorrelation function for Asp 22 was factored into the complete autocorrelation function $C_M(t) \cdot C_f(t) \cdot C_s(t)$. Given that the experimental relaxation values for Asp 22 can be predicted rather well assuming no slow ps–ns internal motion, it is hardly surprising that only a modest proportion of the MD-predicted $C_s(t)$ can be present in spectral densities that accurately predict the experimental rates. In particular, the MD predicted $C_s(t)$ must be scaled down by 85% in order to yield a predicted value equal to the experimental R_1 rate (Fig. 7A). An even lower fraction of the MD predicted $C_s(t)$ autocorrelation function must contribute to predicted R_2 rate if discrepancy with the experimental data is to be reduced below 2% (Fig. 7B).

For two-state transitions, only in the case of a small minor population can the scaling of the estimated $C_s(t)$ contribution be expected to be directly proportionate to the underlying relative population of the two species. As reported by Trbovic, Kim, Friesner and Palmer [37], the nonnative hydrogen bond that stabilizes the minor conformation for Asp 22 is formed 18% of the time in their OPLS-AA simulations, 29% of the time in the ff99SB simulations and 48% of the time in the ff03 simulations. Yet the predicted S^2 values for Asp 22 are near 0.5 for all three force fields. The analysis summarized in Fig. 7 implies that the MD-predicted $C_s(t)$ autocorrelation function for Asp 22 must be attenuated at least 5- to 10-fold to be compatible with the experimental data. These results further imply that if the transitions of this minor species follow the kinetics predicted from the MD simulations, the population of this minor species must be substantially more than 5- to 10-fold below the MD predicted level.

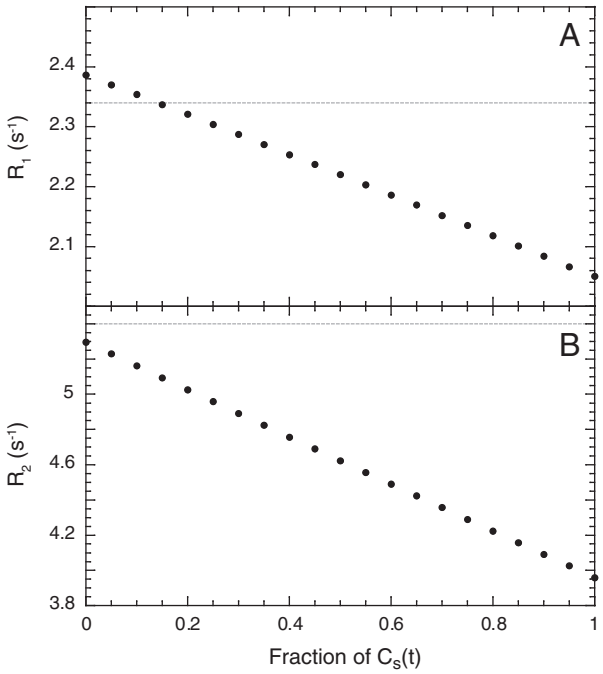

Fig. 7. Prediction of the ^{15}N longitudinal (panel A) and transverse (panel B) relaxation rates for Asp 22 of GB3 as a function of the fraction of the bond vector autocorrelation function contribution arising from slow internal motion as predicted from the RVR-MD analysis. The horizontal lines indicate the experimental values [20].

4. Conclusion

Rotational velocity rescaling for 1 μs of NVE molecular dynamics simulations on the B3 domain of Protein G enables the accurate prediction of the ^{15}N relaxation parameters for the residues involved in the regular secondary structure of this significantly anisotropic macromolecule without recourse to any system-specific adjustable parameters. Given that no assumption of a time-independent rotational diffusion tensor is required, this approach may prove valuable in the analysis of more conformationally disordered molecules. Other techniques that are sensitive to molecular tumbling rates, such as fluorescence depolarization and hydrodynamic modeling, may benefit from the ability to accurately rescale rotational diffusion in MD simulations. In addition to a rotational velocity rescaling factor that corresponds quite closely to that predicted from the elevated self-diffusion rate for the CHARMM-modified TIP3P water model used in the calculations, fitting to the experimental field dependent NMR relaxation measurements on GB3 also provide a powerful test for the optimal values for the average ^{15}N CSA value and $^{1}H-^{15}N$ dipole bond length. The ability of an average ^{15}N CSA value to outperform the experimentally determined residue-specific CSA values for GB3 in predicting NMR relaxation behavior is suggested to arise from the compensating effect on the dipolar coupling that arises from the lengthening of the H – N bond upon hydrogen bond formation. The feasibility of such direct prediction of experimental relaxation data will provide a powerful check for the presence of systematic error in the experimental data. This approach offers a valuable means for not only identifying inaccuracies in force field-based predictions but also for providing estimates for the lower bounds of the resultant errors in relative populations and rates of conformational interchange.

Acknowledgments

We acknowledge the use of the IBM Intelligent Cluster at Union College and the assistance of David Hemmingdinger.

Appendix A. Supplementary data

Supplementary data to this article can be found online at http://dx.doi.org/10.1016/j.bpc.2012.05.005.

References

[1] G. Lipari, A. Szabo, Model-free approach to the interpretation of nuclear magnetic resonance relaxation in macromolecules. 1. Theory and range of validity, Journal of the American Chemical Society 104 (1982) 4546–4559.
[2] G. Lipari, A. Szabo, Model-free approach to the interpretation of nuclear magnetic resonance relaxation in macromolecules. 2. Analysis of experimental results, Journal of the American Chemical Society 104 (1982) 4559–4570.
[3] G.M. Clore, A. Szabo, A. Bax, L.E. Kay, P.C. Driscoll, A.M. Gronenborn, Deviations from the simple 2-parameter model-free approach to the interpretation of N-15 nuclear relaxation of proteins, Journal of the American Chemical Society 112 (1990) 4989–4991.
[4] V.A. Jarymowycz, M.J. Stone, Fast time scale dynamics of protein backbones: NMR relaxation methods, applications, and functional consequences, Chemical Reviews 106 (2006) 1624–1671.
[5] T.I. Igumenova, K.K. Frederick, A.J. Wand, Characterization of the fast dynamics of protein amino acid side chains using NMR relaxation in solution, Chemical Reviews 106 (2006) 1672–1699.
[6] D.T. Woessner, Nuclear spin relaxation in ellipsoids undergoing rotational Brownian motion, Journal of Chemical Physics 37 (1962) 647–654.
[7] V. Wong, D.A. Case, Evaluating rotational diffusion from protein MD simulations, The Journal of Physical Chemistry. B 112 (2008) 6013–6024.
[8] K. Chen, N. Tjandra, Extended model free approach to analyze correlation functions of multidomain proteins in the presence of motional coupling, Journal of the American Chemical Society 130 (2008) 12745–12751.
[9] A. Polimeno, J.H. Freed, Slow motional ESR in complex fluids: the slowly relaxing local structure model of solvent cage effects, Journal of Physical Chemistry 99 (1995) 10995–11006.
[10] Z. Liang, J.H. Freed, An assessment of the applicability of multifrequency ESR to study the complex dynamics of biomolecules, The Journal of Physical Chemistry. B 103 (1999) 6384–6396.
[11] V. Tugarinov, Z. Liang, Y.E. Shapiro, J.H. Freed, E. Meirovitch, A structural mode-coupling approach to ^{15}N NMR relaxation in proteins, Journal of the American Chemical Society 123 (2001) 3055–3063.
[12] M. Zerbetto, M. Buck, E. Meirovitch, A. Polimeno, Integrated computational approach to the analysis of NMR relaxation in proteins: application to ps–ns main chain $^{15}N-^{1}H$ and global dynamics of the rho GTPase binding domain of plexin-B1, The Journal of Physical Chemistry. B 115 (2011) 376–388.
[13] B.R. Brooks, C.L. Brooks, A.D. Mackerell, L. Nilsson, R.J. Petrella, B. Roux, Y. Won, G. Archontis, C. Bartels, S. Boresch, A. Caflisch, L. Caves, Q. Cui, A.R. Dinner, M. Feig, S. Fischer, J. Gao, M. Hodoscek, W. Im, K. Kuczera, T. Lazaridis, J. Ma, V. Ovchinnikov, E. Paci, R.W. Pastor, C.B. Post, J.Z. Pu, M. Schaefer, B. Tidor, R.M. Venable, H.L. Woodcock, X. Wu, W. Yang, D.M. York, M. Karplus, CHARMM: the biomolecular simulation program, Journal of Computational Chemistry 30 (2009) 1545–1614.
[14] C.Y. Lu, D.A. van den Bout, Effect of finite trajectory length on the correlation function analysis of single molecule data, Journal of Chemical Physics 125 (2006) 124701.
[15] J.J. Prompers, R. Brüschweiler, General framework for studying the dynamics of folded and nonfolded proteins by NMR relaxation spectroscopy and MD simulation, Journal of the American Chemical Society 124 (2002) 4522–4534.
[16] S.F. Lienin, T. Bremi, B. Brutscher, R. Brüschweiler, R.R. Ernst, Anisotropic intramolecular backbone dynamics of ubiquitin characterized by NMR relaxation and MD computer simulation, Journal of the American Chemical Society 120 (1998) 9870–9879.
[17] P. Mark, L. Nilsson, Structure and dynamics of the TIP3P, SPC, and SPC/E water models at 298 K, Journal of Physical Chemistry A 105 (2001) 9954–9960.
[18] C. Peter, X. Daura, W.F. van Gunsteren, Calculation of NMR-relaxation parameters for flexible molecules from molecular dynamics simulations, Journal of Biomolecular NMR 20 (2001) 297–310.
[19] P. Maragakis, K. Lindorff-Larsen, M.P. Eastwood, R.O. Dror, J.L. Klepeis, I.T. Arkin, M.Ø. Jensen, H. Xu, N. Trbovic, R.A. Friesner, A.G. Palmer III, D.E. Shaw, Microsecond molecular dynamics simulation shows effect of slow loop dynamics on backbone amide order parameters of proteins, The Journal of Physical Chemistry. B 112 (2008) 6155–6158.
[20] J.B. Hall, D. Fushman, Variability of the ^{15}N chemical shielding tensors in the B3 domain of protein G from ^{15}N relaxation measurements at several fields. Implications for backbone order parameters, Journal of the American Chemical Society 128 (2006) 7855–7870.
[21] L. Yao, A. Grishaev, G. Cornilescu, A. Bax, Site-specific backbone amide ^{15}N chemical shift anisotropy tensors in a small protein from liquid crystal and cross-correlated relaxation measurements, Journal of the American Chemical Society 132 (2010) 4295–4309.
[22] B.J. Wylie, L.J. Sperling, H.L. Frericks, G.J. Shah, W.T. Franks, C.M. Rienstra, Chemical-shift anisotropy measurements of amide and carbonyl resonances in a microcrystalline protein with slow magic-angle spinning NMR spectroscopy, Journal of the American Chemical Society 129 (2007) 5318–5319.
[23] B.J. Wylie, L.J. Sperling, A.J. Nieuwkoop, W.T. Franks, E. Oldfield, C.M. Rienstra, Ultrahigh resolution protein structures using NMR chemical shift tensors,

Proceedings of the National Academy of Sciences of the United States of America 108 (2011) 16974–16979.
[24] L. Cai, D. Fushman, D.S. Kosov, Density functional calculations of chemical shielding of backbone ^{15}N in helical residues of protein G, Journal of Biomolecular NMR 45 (2009) 245–253.
[25] L. Cai, D.S. Kosov, D. Fushman, Density functional calculations of backbone ^{15}N shielding tensors in beta-sheets and turn residues of protein G, Journal of Biomolecular NMR 50 (2011) 19–33.
[26] S. Tang, D.A. Case, Calculation of chemical shift anisotropy in proteins, Journal of Biomolecular NMR 51 (2011) 303–312.
[27] J.P. Derrick, D.B. Wigley, The third IgG-binding domain from streptococcal protein G. An analysis by X-ray crystallography of the structure alone and in a complex with Fab, Journal of Molecular Biology 243 (1994) 906–918.
[28] E.F. Pettersen, T.D. Goddard, C.C. Huang, G.S. Couch, D.M. Greenblatt, E.C. Meng, T.E. Ferrin, UCSF chimera — a visualization system for exploratory research and analysis, Journal of Computational Chemistry 25 (2004) 1605–1612.
[29] W. Humphrey, A. Dalke, K. Schulten, VMD — visual molecular dynamics, Journal of Molecular Graphics 14 (1996) 33–38.
[30] J.C. Phillips, R. Braun, W. Wang, J. Gumbart, E. Taikhorshid, E. Villa, C. Chipot, R.D. Skeel, L. Kale, K. Schulten, Scalable molecular dynamics with NAMD, Journal of Computational Chemistry 26 (2005) 1781–1802.
[31] S.K. Kearsley, On the orthogonal transformation used for structural comparisons, Acta Crystallographica Section A 45 (1989) 208–210.
[32] B. Rupp, S. Parkin, PDBSUP-A FORTRANP Program that Determines the Rotation Matrix and Translation Vector for Best Fit Superposition of Two PDB Files by Solving the Quaternion Eigenvalue Problem, Lawrence Livermore National Laboratory, Livermore, CA, 1996.
[33] D.R. Flower, Rotational superposition: a review of methods, Journal of Molecular Graphics and Modelling 17 (1999) 238–244.
[34] W.H. Press, B.P. Flannery, S.A. Teukolsky, W.T. Vetterling, Numerical Recipes, 1st ed Cambridge University Press, Cambridge, 1989.
[35] J. Cavanagh, W.J. Fairbrother, A.G. Palmer III, N.J. Skelton, Protein NMR Spectroscopy, Principles & Practice, Academic Press, San Diego, CA, 1996.
[36] J.B. Hall, D. Fushman, Characterization of the overall and local dynamics of a protein with intermediate rotational anisotropy: differentiating between conformational exchange and anisotropic diffusion in the B3 domain of protein G, Journal of Biomolecular NMR 27 (2003) 261–275.
[37] N. Trbovic, B. Kim, R.A. Friesner, A.G. Palmer, Structural analysis of protein dynamics by MD simulations and NMR spin-relaxation, Proteins 71 (2008) 684–694.
[38] D.A. Case, Calculations of NMR dipolar coupling strengths in model peptides, Journal of Biomolecular NMR 15 (1999) 95–102.
[39] J.P. Ryckaert, G. Ciccotti, H.J.C. Berendsen, Numerical integration of the Cartesian equations of motion of a system with constraints: molecular dynamics of n-alkanes, Journal of Computational Physics 23 (1977) 327–341.
[40] M. Ottiger, A. Bax, Determination of relative $N-H^N$, $N-C'$, $C^\alpha-C'$, and $C^\alpha-H^\alpha$ effective bond lengths in a protein by NMR in a dilute liquid crystalline phase, Journal of the American Chemical Society 120 (1998) 12334–12341.
[41] B. Vögeli, L. Yao, Correlated dynamics between protein HN and HC bonds observed by NMR cross relaxation, Journal of the American Chemical Society 131 (2009) 3668–3678.
[42] L. Yao, B. Vögeli, J. Ying, A. Bax, NMR determination of amide N–H equilibrium bond length from concerted dipolar coupling measurements, Journal of the American Chemical Society 130 (2008) 16518–16520.
[43] H. Guo, M. Karplus, Ab initio studies of hydrogen bonding of N-methylamide: structure, cooperativity, and internal rotational barriers, Journal of Physical Chemistry 96 (1992) 7273–7287.
[44] P. Damberg, J. Jarvet, A. Gräslund, Limited variations in ^{15}N CSA magnitudes and orientations in ubiquitin are revealed by joint analysis of longitudinal and transverse NMR relaxation, Journal of the American Chemical Society 127 (2005) 1995–2005.
[45] A. Kvick, A.R. Al-karaghouli, T.F. Koetzle, Deformation electron density of α-glycylglycine at 82 K. I. The neutron diffraction study, Acta Crystallographica Section B 33 (1979) 3796–3801.
[46] F. Ferrage, D. Cowburn, R. Ghose, Accurate sampling of high-frequency motions in proteins by steady-state $^{15}N-\{^1H\}$ nuclear Overhauser effect measurements in the presence of cross-correlated relaxation, Journal of the American Chemical Society 131 (2009) 6048–6049.
[47] F. Ferrage, A. Piserchio, D. Cowburn, R. Ghose, On the measurement of $^{15}N-\{^1H\}$ nuclear Overhauser effects, Journal of Magnetic Resonance 192 (2008) 302–313.
[48] F. Ferrage, A. Reichel, S. Battacharya, D. Cowburn, R. Ghose, On the measurement of $^{15}N-\{^1H\}$ nuclear Overhauser effects. 2. Effects of the saturation scheme and water signal suppression, Journal of Magnetic Resonance 207 (2010) 294–303.